IEEE Access
Multidisciplinary | Rapid Review | Open Access Journal

Received December 17, 2020, accepted December 28, 2020, date of publication January 5, 2021, date of current version January 12, 2021.

Digital Object Identifier 10.1109/ACCESS.2021.3049341

Automatic Classification Algorithm for Diffused Liver Diseases Based on Ultrasound Images

AHMED GABER MABROUK[1], ALAA HAMDY[2], HAMMAM M. ABDELAAL[3], AHMED GAMAL ELKATTAN[4], MOTASEM M. ELSHOURBAGY[5], AND HASSAN A. YOUNESS ALANSARY[1], (Member, IEEE)

[1]Department of Computers and Systems Engineering, Faculty of Engineering, Minia University, Minya 61519, Egypt
[2]Department of Communications, Electronics, and Computer Engineering, Faculty of Engineering, Helwan University, Cairo 11795, Egypt
[3]Nuclear Safety Research Center, Egyptian Atomic Energy Authority, Cairo, Egypt
[4]Faculty of Administrative Sciences, King Salman International University, Ras-Sudr 46612, Egypt
[5]Department of Physics and Engineering Mathematics Mattaria, Faculty of Engineering, Helwan University, Cairo 11795, Egypt

Corresponding author: Ahmed Gaber Mabrouk (agaber2008@csi.edu.eg)

ABSTRACT Diffuse liver diseases such as fatty liver and cirrhosis, are leading causes of disability and fatality across the world. Early diagnosis of these diseases is extremely important to save lives and improve the effectiveness of treatment. This study proposes a non-invasive method for diagnosing liver diseases using ultrasound images, by classifying liver tissue as normal, steatosis, or cirrhosis, using feature extraction, feature selection, and classification. First, the correlation, homogeneity, variance, entropy, contrast, energy, long run emphasis, run percentage, and standard deviation are determined. Second, the most efficient features are selected based on the Fisher discriminant and manual selection methods. Third, three voting-based sub-classifiers are used, namely, the normal/steatosis, normal/cirrhosis, and steatosis/cirrhosis classifiers. The final liver tissue classification is based on the majority function. Our classification method provides two key contributions: combination of two different feature selection methods, avoiding the limitations of each method while benefiting from their strengths; and classifier categorization into three sub-classifiers, where the overall classification is based on the decision of each individual sub-classifier. We obtained recognition accuracies for the normal/steatosis, normal/cirrhosis, and steatosis/cirrhosis classifiers as 95%, 95.74%, and 94.23%, respectively, and an overall recognition accuracy of 95%, which outperforms other methods.

INDEX TERMS Feature extraction, Fisher discriminant, region of interest, majority based classifier, liver diseases.

I. INTRODUCTION

Early diagnosis is vital in treating a disease. Diagnosis relies on the skills, experience, and knowledge of the practising physicians, although human errors may sometimes occur. Recently, various artificial intelligence-based methods are being increasingly used for liver disorder diagnosis to assist doctors in the diagnosis of patients. Extended cirrhosis and steatosis liver disease may cause the appearance of malignant or benign tumours in the liver. Any abnormality in the liver adversely affects the rest of the body, as well as the general health of the patient [1]–[3].

Fatty liver disease (FLD) occurs when the human body produces a considerable amount of fat or does not efficiently metabolize fat. This excess fat is stored in the liver cells, where it accumulates triglycerides in the blood, causing FLD [4]. It is believed that FLD involves the pathogenesis of various common disorders, such as Type II diabetes and cardiovascular diseases. A steatosis condition can progress to advanced stages with fibrosis and non-alcoholic steatohepatitis (NASH), increasing the risk of hepatocellular carcinoma and cirrhosis [5].

Cirrhosis is an advanced stage of liver fibrosis and is caused by many types of liver diseases and conditions, such as chronic alcoholism and hepatitis. As cirrhosis progresses, more scar tissue forms, making it difficult for the liver to function, and advanced cirrhosis is life-threatening. However, if liver cirrhosis is diagnosed early, the causes can be treated, avoiding further damage, and its progression can be reduced, or in rare cases, reversed. The most common causes of cirrhosis are HCV, Hepatitis B virus (HBV) and HCV are the most common causes of liver diseases in the developing world [6], [7]. Patients with pre-existing liver cirrhosis conditions may be more susceptible to SARS-CoV-2 coronavirus (COVID-19) infection because of their systemic immunocompromised condition [8].

The associate editor coordinating the review of this manuscript and approving it for publication was Jon Atli Benediktsson.

There are two methods of diagnosis and identification for liver diseases. The first is an invasive method, such as liver biopsy. Liver biopsy is one of the most efficient techniques employed because of its accuracy. However, liver biopsy has some associated disadvantages, which include its invasiveness, mortality caused by bleeding, and some complications such as accidental injury to a nearby organ and pain after undergoing the procedure [9]–[12].

The second method is non-invasive. There are many non-invasive imaging techniques, such as computerized tomography (CT) scanning, magnetic resonance imaging (MRI) scanning [12], and ultrasound (US) scanning [4], [10], which are used for liver disease detection. CT is constrained by the inaccurate quantification of steatosis, radiation exposure, and low sensitivity in the case of mild steatosis. MRI-estimated proton density fat fraction (MRI-PDFF) has been demonstrated to correlate with the histology-determined fatty grade in adults with FLD, and magnetic resonance spectroscopy (MRS) has emerged as the leading non-invasive modality for steatosis quantification of FLD in terms of specificity, sensitivity, and reliability [13]. However, MRI and liver biopsies are both expensive and uncommon procedures [12].

Nevertheless, an image-acquisition US device is simple to operate, movable, radiation-free, inexpensive, and available in a wide range of health clinics and radiology centres [13]. One of the major limitations related to using US is the low quality of the acquired images compared to those of CT and MRI. This renders the task of classification extremely difficult and is one of the challenges addressed in this study.

II. RELATED WORKS

In [14], a technique named ultrasound-induced thermal strain imaging (US-TSI) was presented. US-TSI is used to estimate fat content in ex-vivo mouse liver by using the proposed speed temperature theory. As demonstrated in [15], a combination of Discrete Wavelet Transformation (DWT) and contrast enhancement for speckle noise removal from a dataset of 30 cirrhosis and 25 normal liver images was used. K-means clustering with a minimum Euclidian distance followed by artificial neural networks (ANNs) was employed. A study by [16] provides a survey of the machine learning techniques used in diagnosing various diseases. Diffused liver diseases such as fatty liver, hepatitis, and cirrhosis are leading causes of fatality and disability worldwide. As a speckle is present in the high-frequency components of a US image, 2D WPT, which is considered as a richer space-frequency multiresolution analysis scheme, may offer an appropriate texture descriptor. The multi-resolution fractal analysis can add more data regarding the signal heterogeneity. The mean of grey-levels and grey level run length matrix (GLCM) correlation can show variations in granularity between the hepatocellular carcinoma (HCC) and the cirrhotic liver [17]. However, the accuracy of US-based diagnosis depends significantly on the expertise of radiologists. Computer-aided diagnosis (CAD) systems based on US imaging assist in quick diagnosis, provide a reliable ''second evaluation'' for specialists, and act as effective tools for measuring the response of treatment on the patients undergoing clinical trials [10].

A study by [18] developed a technique to distinguish fatty, cirrhotic, and hepatomegaly livers. The grey-level run length matrix (GLRLM), intensity histogram, and GLCM were extracted and used in a multilayer perceptron (MLP). Therefore, an accuracy greater than 90% was obtained. In [19], a texture analysis technique known as texture feature co-occurrence matrix (TFCOM) was proposed to categorize hepatitis, normal, and cirrhotic livers. An accuracy of 86.7% was obtained using the maximum likelihood classifier. In [20], three strategies to classify normal and fatty liver were presented. First, textural features were analysed, and the use of classifier fusion provided an accuracy of 79%. Second, the hepatorenal coefficient (HC) was calculated, followed by statistical analysis. A sensitivity of 90% and specificity of 88% were obtained. Third, the acoustic attenuation coefficient (AAC) was calculated. The author observed that the HC was not influenced by the US machine parameters.

In previous works [4], [15], [18]–[20] the available database was insufficient and considered only two classes: normal/ cirrhosis or normal/steatosis, and none of them adopted the classification of steatosis/cirrhosis. In this study, liver tissues are classified as normal, steatosis, and cirrhosis. It should be mentioned that three radiologists labelled the dataset in order to avoid the incorrect classification.

The rest of this paper is organized as follows: in Section 2, the materials and methods used are described. Section 3 presents the experimental results. Finally, the conclusions are presented in Section 4.

III. MATERIALS AND METHODS

A. IMAGE ACQUISITION

In this study, image acquisition is performed using a GE Logiq p5 US system. Images have been acquired at ''*Elrouad Radiography Center, Menouf city, Egypt*'' by professional medical radiologists and experts. The transmitting frequency of the ultrasound was a 4 MHz with a convex probe.

The challenge in this study is that the use of GE Logiq p5 equipment leads to the acquisition of images with a lower quality in comparison to that obtained with other US equipment (e.g., GE Logiq p9 and Toshiba SSA-700A equipment). We use the GE Logiq p5 as it is one of the most commonly used types of equipment because of its cost effectiveness.

The size of the acquired image is 684 $\times$ 552 pixels. A total of 279 images was collected. An image is acquired from each patient. According to the decisions of the physicians, 95 images are manually categorized as normal, and 105 images are classified as steatosis. The rest of the images (79 images) are classified as cirrhosis.

This study focuses on differentiating between normal/steatosis, normal/cirrhosis, and steatosis/cirrhosis liver based on image analysis. Figure 1 shows an example image for each of the tissue classifications of normal, steatosis, and cirrhosis.

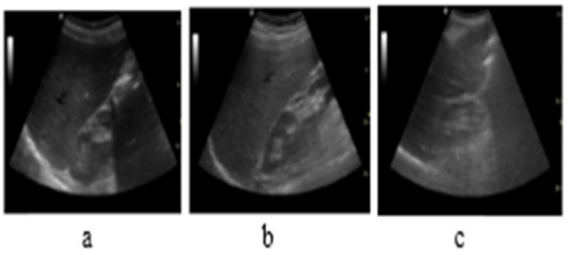

FIGURE 1. Examples of the acquired images a) normal b) steatosis c) cirrhosis.

B. METHODOLOGY

Firstly, multiple regions of interest (ROI) are selected within the liver tissue instead of using single ROI to enhance the performance of the liver diseases diagnosis. Three types of selection parameters are used:

1) SIZE OF EACH ROI

To accurately diagnose the diffused liver disease, a dynamic-sized ROI (rows x columns) is proposed. This is because static-sized ROIs may not contain sufficient information. The dynamic size is determined automatically via a genetic algorithm (GA).

2) NUMBER OF ROIs

Multiple ROIs (1–9 ROIs) are selected and distributed within the liver tissue, according to the guidance of three radiologists. This is also automatically determined by the GA.

3) POSITION OF EACH ROI

The position is determined initially and marked manually by three experienced doctors. Once the ROIs are marked, the fixed positions are used for any newly acquired image.

Secondly, to speed up the processing, only ROIs are transformed from red, green, and blue (RGB) colours to a grey-level.

Thirdly, the features of each ROI are extracted. Instead of the features used in [24], [25], only nine low-computation features including correlation, homogeneity, entropy, variance, energy, contrast, long run emphasis, run percentage, and standard deviation are extracted. Table 1 shows a description of these features [4], [26].

Fourthly, feature selection is used to minimize the number of features. In this study, the Fisher discriminant (F-ratio) is used to reduce the use of nine features to only six features [27] as shown in Fig. 2. This significantly reduces the number of computations, it has been experimentally determined from [28]. Finally, the majority-based classifier is used to identify the category of a liver tissue as normal/steatosis, normal/cirrhosis, and steatosis/cirrhosis liver images.

C. CLASSIFICATION OF TISSUES AS NORMAL/STEATOSIS

In this section, we describe the classification of each selected ROI as normal or steatosis tissue. It was observed that the normal liver has a homogeneous grey level. Otherwise, it would be considered to be a steatosis liver.

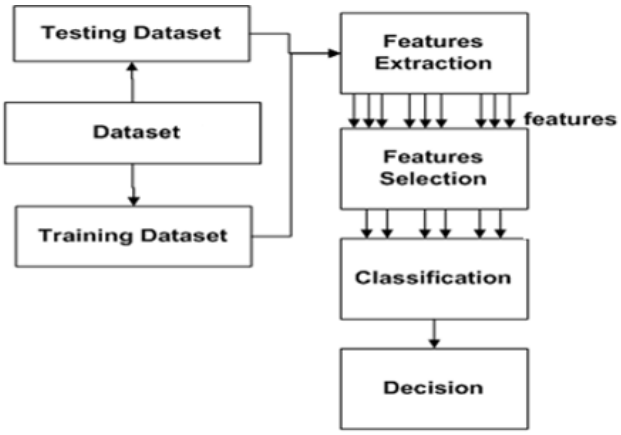

FIGURE 2. Flow diagram illustrating the proposed system.

TABLE 1. Summary of feature equations.

Features	Equation
Correlation (Cor)	$\text{Cor} = \frac{\sum_{i=0}^{G-1}\sum_{j=0}^{G-1}(i \times j) \times P(i,j) - \{u_x \times u_y\}}{\sigma_x \times \sigma_y}$
Homogeneity (Homo)	$\text{Homo} = \sum_{j=0}^{2G-2} \frac{1}{1+j^2}\text{Hd}(j \mid \Delta x, \Delta y)$
Entropy (Ent)	$\text{Ent} = -\sum_{i=0}^{G-1}\sum_{j=0}^{G-1} p(i,j) * \log(p(i,j))$
Variance (Var)	$Var = \sum_{i=0}^{G-1}\sum_{j=0}^{G-1}(i-\mu)^2 \text{P}(i,j)$
Energy (Ene)	$Ene = \sum_{i=0}\sum_{j=0} \text{N}_d^2(i,j)$
Contrast (Con)	$\text{Con} = \sum_{n=0}^{G-1} n^2 \{\sum_{i=1}^{G}\sum_{j=1}^{G} P(i,j)\}, \lvert i-j \rvert = n$
Long run emphasis (LRE)	$LRE = \sum_{i=1}^{G}\sum_{j=1}^{R} j^2(i,j\backslash\theta) / \sum_{i=1}^{G}\sum_{j=1}^{R} P(i,j\backslash\theta)$
Run percentage (RP)	$RP = \frac{1}{N}\sum_{i=1}^{G}\sum_{j=1}^{R} P(i,j\backslash\theta)$
Standard deviations	$\sigma_x = \sum_{i=0}^{\text{Ng}-1}\sum_{j=0}^{Ng-1}(i-u_x)^2 \times \text{P}(i,j), \quad for\ Columns$ $\sigma_y = \sum_{i=0}^{\text{Ng}-1}\sum_{j=0}^{Ng-1}(j-u_y)^2 \times \text{P}(i,j), for\ Rows$

However, it is better to be able to select these thresholds automatically. In this study, a GA is used to optimize the selection of the thresholds.

Additionally, to enhance the recognition rate in this study, other parameters are proposed. Instead of counting the number of decisions by incrementing one to the voting count, the count is increased using the weight factor. This weight factor can be equal to two, three, or more. This is equivalent to increasing the weight of the decision that is made by an experienced doctor. In other words, the weight of an inexpe-

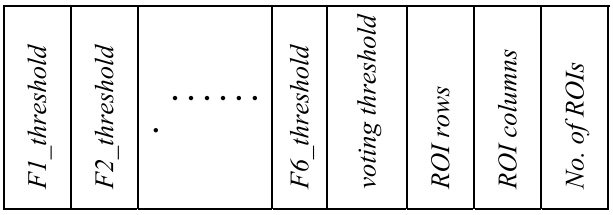

FIGURE 3. Chromosome structure. Feature1 (F1) and etc.

rienced doctor is one, as expressed in the following equation:

$$\text{voting} + 1 \rightarrow \text{voting}. \tag{1}$$

Hence, (1) is modified as follows:

$$\text{voting} + \text{contrast\_weight} \rightarrow \text{voting} \tag{2}$$
$$\text{voting} + \text{variance\_weight} \rightarrow \text{voting}. \tag{3}$$

Therefore, two weight factors are added to the parameters, indicating one weight factor for each extracted feature.

In this study, a voting function is used to identify the type of liver. Further, a voting threshold is used to determine the minimum number of ROIs to classify a given liver as normal. To avoid the manual selection of the thresholds and other parameters mentioned previously, a GA is used.

GA is an adaptive heuristic search algorithm. In GA, firstly, an initial population is formed. The population is composed of 100 chromosomes. Each chromosome is composed of concatenated thresholds or candidate solutions. The chromosome structure is illustrated in Fig. 3. Secondly, each pair of parent chromosomes is selected. Thereafter, the crossover operation is performed at a random crossover point. Thirdly, the mutation operation is performed on each chromosome at a random point. Thereafter, the offspring is generated. Finally, the parent chromosomes and offspring are evaluated using an objective function.

An objective function provides the number of incorrectly classified images. In other words, the objective function in the optimization process is used to maximize the correctly classified images or to minimize the number of incorrectly classified images. The objective function is the reciprocal of the penalty value or specifically, the number of incorrectly classified images.

Figure 4 shows the training and testing phases for optimizing ROI selection using a genetic algorithm. In the training phase, each image of the normal/steatosis liver in the training set is applied to the proposed system. Thereafter, the thresholds, weights, and parameters are automatically selected such that the image is classified as a normal/steatosis case, respectively.

In the testing phase, each image of the testing set is applied to the proposed study. Thereafter, according to the majority function, the liver tissue is classified as normal/steatosis liver. Figure 5 shows the proposed algorithm of the overall process.

D. CLASSIFICATION OF TISSUE AS NORMAL/CIRRHOSIS

For the process of classifying the tissue, each selected ROI is classified as normal or cirrhosis tissue. It is observed that the normal liver has a homogeneous grey level and is characterized by low contrast as well as low variance. Otherwise, it would be considered as a cirrhosis liver. The algorithm in Fig. 5 is applied again by replacing (normal and abnormal) with (normal and cirrhosis).

E. CLASSIFICATION OF TISSUE AS STEATOSIS/CIRRHOSIS

In this process, each selected ROI is classified as a steatosis or cirrhosis tissue. The classification process mentioned in Sections *C* and *D* will be repeated for all the ROIs. Comparing the number of ROIs classified as steatosis livers to the number of ROIs classified as cirrhosis livers, a majority function is used to identify the category of the liver case. In the same way, GA is applied to automatically determine the values of the parameters. The algorithm in Fig. 5 is applied again by replacing (normal and abnormal) with (steatosis and cirrhosis).

F. CLASSIFICATION OF TISSUE AS NORMAL/CIRRHOSIS

In this process, each selected ROI is classified as a normal, steatosis or cirrhosis tissue. It is observed that the process of differentiating between the three classes is quite challenging. To automatically differentiate between the three classes, the previous classification between normal/steatosis, normal/cirrhosis and steatosis/cirrhosis was performed individually (i.e., the test image is applied to each classifier described in Sections *C*, *D* and *E*), as shown in Fig. 6. Thereafter, a majority function is used to select the maximum count.

In other words, to make the correct decision, the opinion of three doctors is taken. The first doctor is specialized in discriminating between normal and steatosis livers. The second doctor is specialized in discriminating between normal and cirrhosis livers, whereas the third doctor is specialized in discriminating between steatosis and cirrhosis livers. The final decision will be taken according to the opinions of the three doctors.

IV. RESULTS AND DISCUSSION

In this study, several experiments were performed. Multiple ROIs of a maximum of nine ROIs for each US image were used. The total ROIs in the normal, steatosis, and cirrhosis liver categories were 855 ($= 95 \times 9$), 945 ($= 105 \times 9$), and 711 ($= 79 \times 9$), respectively.

Figure 7(a) shows the original images acquired using the GE Logiq p5 US machine. The dataset was collected from 279 subjects: 95 normal, 105 liver steatosis, and 79 cirrhosis of known pathology. The images were then converted to greyscale, as shown in Fig. 7(b). The selection of multiple ROIs from ultrasonic images as shown in Fig. 7(c) was performed under the guidance of doctors specialised in treating liver diseases.

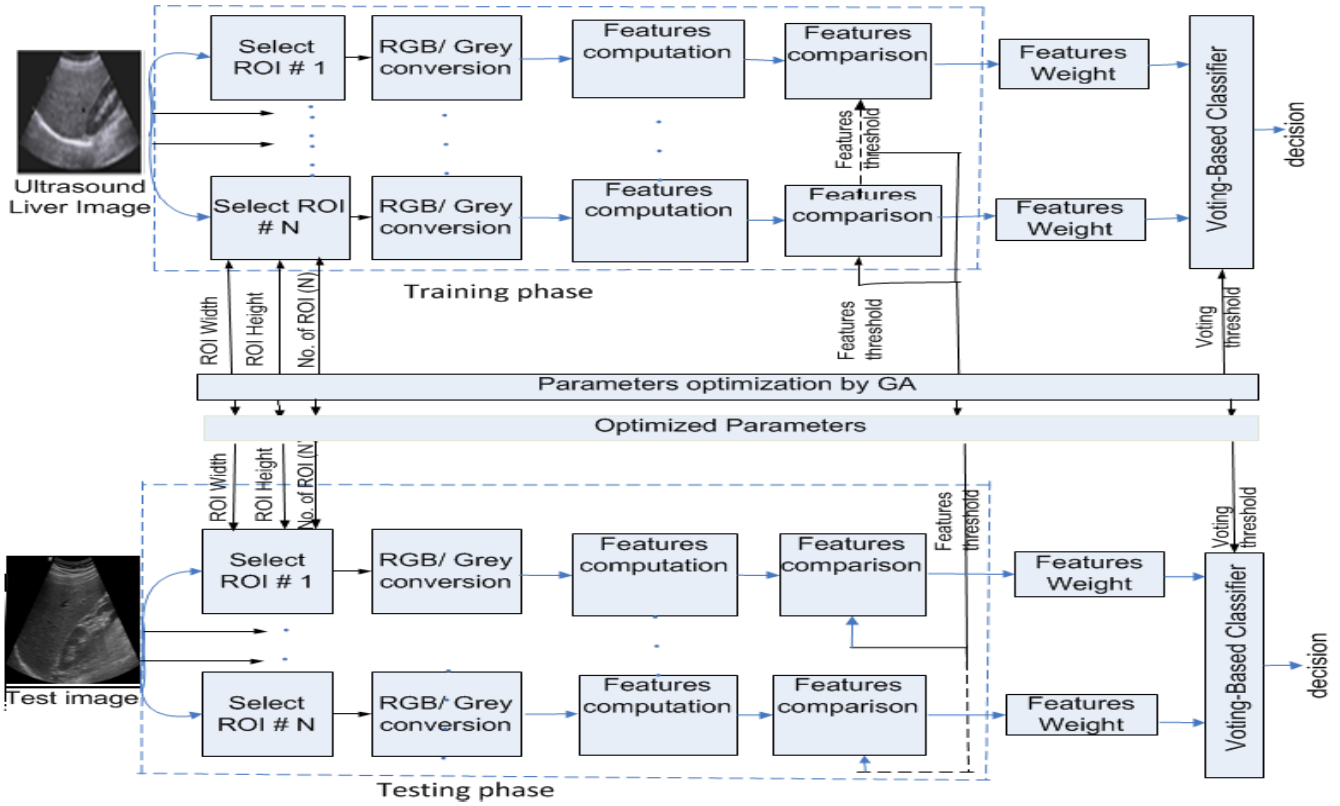

FIGURE 4. Optimizing ROI selection using a genetic algorithm.

TABLE 2. Fisher discriminant of each extracted feature.

Extracted feature	F-ratio
Correlation	6
Homogeneity	4.67
Entropy	4
variance	2.33
Contrast	2
Energy	2
Long run emphasis	1.69
Run percentage	0.81
Standard deviation	0.78

TABLE 3. Recognition rate in case of extracting each feature individually.

Extracted feature	Recognition rate
Contrast	67.4%
Variance	69.7%
Entropy	62.6%
Homogeneity	63.8%
Correlation	65%
Energy	63.8%

The feature selection process is divided into two parts. The first part is determining the Fisher discriminant or F-ratio, which is defined in the following equation [21], [22]:

$$f = \frac{(\mu_1 - \mu_2)^2}{\sigma_1^2 + \sigma_2^2} \tag{6}$$

where μ_1 and μ_2 are the mean values of the two classes, and σ_1^2 and σ_2^2 are the variances of the two classes. Table 2 shows the computed F-ratio of each extracted feature.

The second part of the feature selection process is based on manual selection to determine the most efficient feature. The manual selection is essential in order to verify the experimental result of the Fisher discriminant. During this process, each feature is selected and tested individually. The experimental results show that the variance and the contrast individually achieved the two highest recognition rates compared to the rest of the extracted features (homogeneity, entropy, energy, and correlation), as shown in Table 3.

It is noted that where two features are combined (e.g., contrast and variance), the recognition rate can be increased, as shown in Table 4, compared to the case where these features are used individually (see Table 3). It should be noted that the highest recognition rate in Table 3 is 69.7%, whereas in Table 4, it is 80.5%.

The experimental results show that combining the three features does not lead to a significant improvement in the recognition rate compared to the use of only two features. The dataset is divided into two sets: a training set and a testing set.

A training set of 40 normal, 40 steatosis, and 40 cirrhosis livers is used to train the system, while a testing set of 55 normal images, 65 steatosis images, and 39 cirrhosis liver images is used to enhance the success rate of the classifier. Finally, all the US images are classified (one of the three

```
Algorithm: Optimization of the number of ROIs, ROI size selection,
variance threshold, variance weight, contrast threshold, contrast weight, and
voting threshold

1. For iteration number = 1,2,3,……,number of iteration, do
2. For every chromosome do
    Number of incorrectly classified image = 0
    For every training image do
        voting = 0
        For every ROI of size, m x n do
            Convert ROI into grey level using equation (4)
                I = 0.2989 * R + 0.5870 * G + 0.1140 * B          (4)
            Compute All Features
            If All Features < All Features _threshold
              voting + All Features _weight → voting               (5)
            End if
        End for

        If voting > voting_threshold
            If training image = abnormal
                Number of incorrectly classified image +1→
                Number of incorrectly classified image
            End if
        Else
            If training image = normal
              Number of incorrectly classified image +1→
                    Number of incorrectly classified image
            End if
        End  if
      End for
      Assign fitness score to the chromosome
    End for
  End for

3. For every testing image do
     voting = 0
     For every ROI do
     Convert ROI into grey level f using equation (4)
     Compute All Features using equation (5)

     If All Features < All Features _threshold
          voting + All Features_weight → voting
     End if
   End for

4. If voting > voting_threshold
       Liver case = normal
     Else
       Liver case = Abnormal
     End if
End for
```

FIGURE 5. Parameter optimization using a genetic algorithm.

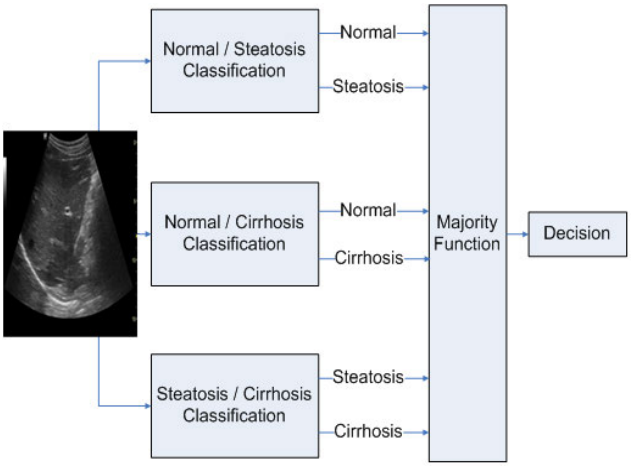

FIGURE 6. Overall flow diagram describing the proposed system.

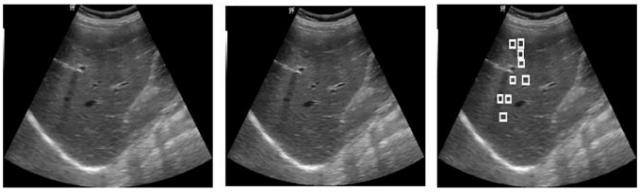

a b c

FIGURE 7. (a) Original acquired image, (b) grey-level image, and (c) grey-level image with multiple ROIs.

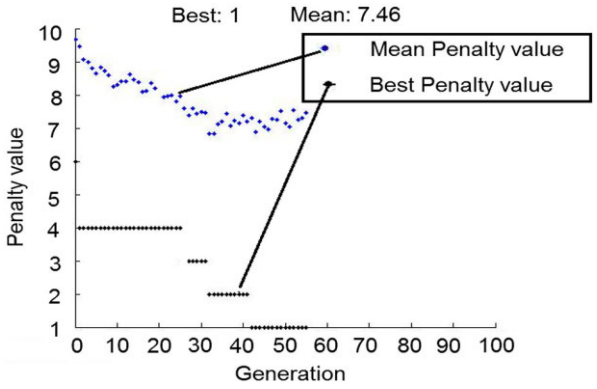

FIGURE 8. Plot of penalty value with varying generation number. The nine parameters are optimized to increase the number of correctly classified images.

pathologies: normal, cirrhotic and steatosis liver diseases) manually by two specialist physicians.

The generation increases with decreasing number of incorrectly classified images or false negatives, as shown in Fig. 8.

Table 5 shows that the use of weighting leads to a significant improvement in the recognition rate, where the recognition rate increases by 10%. From the obtained experimental results in [23], weighting is recommended.

Considering a normal/steatosis classifier, the proposed algorithm in Section *C* achieves a recognition rate of 95% with GA and 66.7% without GA, as shown in Table 6.

Moreover, considering a normal/cirrhosis classifier, the proposed algorithm in Section *D* achieves a recognition rate of 95.74% with GA and 61.1% without GA. For a steatosis/cirrhosis classifier, the proposed algorithm in Section *E* achieves a recognition rate of 94.23% with GA and 63.2% without GA. For a normal/steatosis/cirrhosis classifier, the proposed algorithm in Section *F* achieves a recognition rate of 95% with GA and 63.6% without GA, as shown in Table 6.

Table 7 illustrates the confusion matrix of the three classes to identify the no of samples that belong to each class (Normal, Steatosis, and Cirrhosis). Each row of the matrix represents the no of instances in an actual class while each column represents the no of instances in a predicted class.

Table 8 shows the results of each classifier for selected test images. For instance, considering normal image 1 (Nom_Img1), the normal/steatosis classifier classifies it as normal liver (Nom), the normal/cirrhosis classifier also classifies it as normal liver (Nom), whereas the steatosis/cirrhosis

TABLE 4. Recognition rate in percentage in case of selecting two features.

Extracted feature	Recognition rate
Contrast & Variance	80.5
Contrast & Entropy	66.4%
Contrast & Homogeneity	65.2%
Contrast & Correlation	67.5%
Contrast & Energy	64%
Variance & Entropy	67.5%
Variance & Homogeneity	66.4%
Variance & Correlation	68.7%
Variance & Energy	65.2%
Entropy & Homogeneity	62.8%
Entropy & Correlation	65.2%
Entropy & Energy	61.6%
Homogeneity & Correlation	64%
Homogeneity & Energy	61.6%
Correlation & Energy	62.8%

TABLE 5. Recognition rate in the training and testing phases with/without weighting in case of extracting two features (with feature selection).

	Without weighting %	With weighting %
Training set	88	98.6
Testing set	75.6	95

TABLE 6. Recognition rate of normal/steatosis, normal/cirrhosis, steatosis/cirrhosis and normal/steatosis/cirrhosis classifiers.

Recognition rate	normal/steatosis	normal/cirrhosis	steatosis/cirrhosis	normal/steatosis/cirrhosis
Training set Without GA	70%	80%	65%	65%
Training set With GA	98.7%	100%	95%	97.9%
Testing set Without GA	66.7 %	61.1%	63.2%	63.6%
Testing set With GA	95%	95.74%	94.23%	95%

TABLE 7. The overall confusion matrix.

For testing datasets	Normal	Steatosis	Cirrhosis
Normal (55)	52	3	0
Steatosis(65)	3	60	2
Cirrhosis (39)	0	1	38

classifier classifies it as cirrhosis liver (Cirr). Consequently, the final decision for this test image based on the majority function will be normal (Nom). This is a correct classification.

Considering steatosis image 4 (st_Img4), the normal/steatosis classifier classifies it as steatosis liver (St), the normal/cirrhosis classifier classifies it as cirrhosis liver (Cirr), and the steatosis/cirrhosis classifier classifies it as cirrhosis liver (Cirr). Consequently, the final decision for this test image based on the majority function will be cirrhosis (Cirr), and this is an incorrect classification.

Table 9 presents a comparison between the proposed system and a previous method. It should be noted that the US system used in this study produces poor quality images compared to other studies. However, the proposed system achieved better accuracy compared to other researches except for [26] which used a higher resolution US machine but had the same accuracy (95%) as this study. It should be mentioned that the proposed system discriminates between steatosis and cirrhosis. However, no other researches discriminate between these two classes. Another advantage of the proposed system is the simplicity achieved via building the whole complicated classifier using simple sub classifiers with the majority function.

TABLE 8. Result of liver tissue classification.

Test images	Nom./ St.	Nom./ Cirr.	St./ Cirr.	Majority Function
Nom_Img1	Nom	Nom	Cirr	**Nom**
Nom_Img2	Nom	Nom	St	**Nom**
Nom_Img3	Nom	Nom	Cirr	**Nom**
Nom_Img4	Nom	Nom	St	**Nom**
St_Img1	St	Cirr	St	**St**
St_Img2	St	Cirr	St	**St**
St_Img3	St	Cirr	St	**St**
St_Img4	St	Cirr	Cirr	**Cirr**
St_Img5	Nom	Cirr	St	**Unknown**
Cirr_Img1	St	Cirr	Cirr	**Cirr**
Cirr_Img2	St	Cirr	Cirr	**Cirr**
Cirr_Img3	St	Cirr	Cirr	**Cirr**
Cirr_Img4	Nom	Nom	St	**Nom**

*image (Img), Normal (Nom), Steatosis (St), Cirrhosis (Cirr)

TABLE 9. Comparison between previous works and the proposed work.

Author	US/classes (No. of Patients)	Features/classifier	performance
[2]	normal, fatty	Texture, wavelet transform, and HOS/DT and FSC	Accuracy: 93.3%
[25]	Normal and fatty (177 echo-graphic images) obtained from 36 patients	FOS, GLRLM, GLCM, law's texture energy and fractal dimension/ and three classifiers; ANN, SVM & KNN ANN, SVM & KNN	Accuracy: 76.9% 79.7% 74.1% respectively
[18]	normal (30), fatty (10), cirrhosis (10), hepatomegaly (10)	Intensity histogram, GLCM, GLRLM, Invariant moments/BPNN	Accuracy: 92.5%
[20]	normal (68), Fatty (52)	FOS, GLCM, GLRLM, Gabor filter, Laws' filter, fractal dimension, lacunarity, hepatorenal coefficient, attenuation/ANN, SVM, k-NN, Bayes, Decision Tree	classifiers fusion: 79%
[26]	normal (80), Fatty (100)	Texture features/Information fusion-based classifier	Accuracy: 95%
[24]	Normal(28), steatosis(47), fibrosis(42), and cirrhosis(12) images	GLCM and Wavelet Packet Transform (WPT)/SVM	Accuracy: 94.91%
Proposed work	normal/steatosis normal/cirrhosis: steatosis/cirrhosis:	6 Features/Majority Function	Accuracy: 95% Accuracy:95.74% Accuracy: 94.23% respectively

V. CONCLUSION

In this study, a diagnostic method for diffused liver tissues is proposed. The unenhanced US images of liver tissues are classified as normal, steatosis, or cirrhosis. The US images (acquired via a non-invasive method) are used for the identification and diagnosis of normal and abnormal liver tissue.

Individual classifications between normal/steatosis, normal/cirrhosis and steatosis/cirrhosis are achieved. The recognition accuracy for normal/steatosis classifier is 95%, that of normal/cirrhosis classifier is 95.74%, and that of steatosis/cirrhosis classifier is 94.23%. The final decision is based on the majority function. The recognition accuracy achieved is 95%.

The proposed system has the potential to be used in hospitals and clinics to assist in the evaluation of liver diseases in real-time. Therefore, it is expected to reduce the workload of radiologists because they do not need to manually segment the ROI. Moreover, the proposed system can be adopted to characterize the various stages of diffused liver fibrosis.

A limitation of this study is that there is no publicly available database that can be used to further verify the method. Furthermore, the poor quality of the US images leads to a demand for more enhanced techniques or efficient features without degrading the image information. As a future work, the recognition accuracy of the proposed system could be improved by decreasing the rate of false-negative (FN) cases to allow us to better differentiate between closely resembling diseases.

ACKNOWLEDGMENT

The authors would like to thank ''El-Rouadscan Center–Menouf city-Elmenofia-Egyptian Ministry of Health'' for kindly providing the ultrasound images used in this study. They would also like to thank Dr. A. Fouad Yonis–Managing Director of El-Rouadscan Center, Dr. A. Elpeltagy and Dr. Asmaa Wagih–specialized in analyzing medical images–for their valuable guidance in the work.

Finally, they would like to acknowledge the invaluable contributions extended by the El-Rouadscan team members for their medical field knowledge support.

REFERENCES

[1] D. Suma, A. Vysakh, and M. Latha, ''Molecular pathways in non-alcoholic fatty liver disease: An emerging menace,'' *Austin Hepatology*, vol. 2, no. 1, p. 1005, 2017.

[2] U. R. Acharya, J. E. W. Koh, Y. Hagiwara, J. H. Tan, A. Gertych, A. Vijayananthan, N. A. Yaakup, B. J. J. Abdullah, M. K. B. M. Fabell, and C. H. Yeong, ''Automated diagnosis of focal liver lesions using bidirectional empirical mode decomposition features,'' *Comput. Biol. Med.*, vol. 94, pp. 11–18, Mar. 2018.

[3] N. Chalasani, Z. Younossi, J. E. Lavine, M. Charlton, K. Cusi, M. Rinella, S. A. Harrison, E. M. Brunt, and A. J. Sanyal, ''The diagnosis and management of nonalcoholic fatty liver disease: Practice guidance from the American association for the study of liver diseases,'' *Hepatology*, vol. 67, no. 1, pp. 328–357, Jan. 2018.

[4] K. Raghesh Krishnan and S. Radhakrishnan, ''Hybrid approach to classification of focal and diffused liver disorders using ultrasound images with wavelets and texture features,'' *IET Image Process.*, vol. 11, no. 7, pp. 530–538, Jul. 2017.

[5] N. Stefan, H.-U. Häring, and K. Cusi, ''Non-alcoholic fatty liver disease: Causes, diagnosis, cardiometabolic consequences, and treatment strategies,'' *Lancet Diabetes Endocrinology*, vol. 7, no. 4, pp. 313–324, Apr. 2019.

[6] J. Tao, W. Zhang, H. Yue, G. Zhu, W. Wu, W. Gong, H. Fang, G. He, X. Hu, H. Zhao, and A. Liu, ''Prevalence of hepatitis B virus infection in Shenzhen, China, 2015–2018,'' *Sci. Rep.*, vol. 9, no. 1, pp. 1–9, 2019.

[7] D. Maucort-Boulch, C. de Martel, S. Franceschi, and M. Plummer, ''Fraction and incidence of liver cancer attributable to hepatitis b and c viruses worldwide,'' *Int. J. Cancer*, vol. 142, no. 12, pp. 2471–2477, Jun. 2018.

[8] C. Zhang, L. Shi, and F.-S. Wang, ''Liver injury in COVID-19: Management and challenges,'' *Lancet Gastroenterology Hepatology*, vol. 5, no. 5, pp. 428–430, May 2020.

[9] P. Bharti, D. Mittal, and R. Ananthasivan, ''Computer-aided characterization and diagnosis of diffuse liver diseases based on ultrasound imaging: A review,'' *Ultrason. Imag.*, vol. 39, no. 1, pp. 33–61, Jan. 2017.

[10] U. R. Acharya, O. Faust, F. Molinari, S. V. Sree, S. P. Junnarkar, and V. Sudarshan, ''Ultrasound-based tissue characterization and classification of fatty liver disease: A screening and diagnostic paradigm,'' *Knowl.-Based Syst.*, vol. 75, pp. 66–77, Feb. 2015.

[11] L. Petitclerc, G. Sebastiani, G. Gilbert, G. Cloutier, and A. Tang, ''Liver fibrosis: Review of current imaging and MRI quantification techniques,'' *J. Magn. Reson. Imag.*, vol. 45, no. 5, pp. 1276–1295, May 2017.

[12] D. Larrey, L. Meunier, and J. Ursic-Bedoya, ''Liver biopsy in chronic liver diseases: Is there a favorable benefit: Risk balance?'' *Ann. Hepatology*, vol. 16, no. 4, pp. 487–489, Jul. 2017.

[13] S. C. Lin, E. Heba, T. Wolfson, B. Ang, A. Gamst, A. Han, J. W. Erdman Jr, W. D. O'Brien Jr, M. P. Andre, and C. B. Sirlin, ''Noninvasive diagnosis of nonalcoholic fatty liver disease and quantification of liver fat using a new quantitative ultrasound technique,'' *Clin. Gastroenterol. Hepatol.*, vol. 13, no. 7, pp. 1337–1345, Jul. 2015.

[14] A. M. Mahmoud, X. Ding, D. Dutta, V. P. Singh, and K. Kim, ''Detecting hepatic steatosis using ultrasound-induced thermal strain imaging: An *ex vivo* animal study,'' *Phys. Med. Biol.*, vol. 59, no. 4, p. 881, 2014.

[15] V. V. Hambire and S. Ganorkar, ''Classification of liver disease based on US images,'' *Int. Res. J. Eng. Technol.*, vol. 4, no. 4, 2015.

[16] G. Kumar and R. Kalra, ''A survey on machine learning techniques in health care industry,'' *Int. J. Recent Res. Aspects*, vol. 3, no. 2, pp. 128–132, 2016.

[17] C.-C. Wu, W.-L. Lee, Y.-C. Chen, C.-H. Lai, and K.-S. Hsieh, ''Ultrasonic liver tissue characterization by feature fusion,'' *Expert Syst. Appl.*, vol. 39, no. 10, pp. 9389–9397, Aug. 2012.

[18] K. Kalyan, B. Jakhia, R. D. Lele, M. Joshi, and A. Chowdhary, ''Artificial neural network application in the diagnosis of disease conditions with liver ultrasound images,'' *Adv. Bioinf.*, vol. 2014, pp. 1–15, Sep. 2014.

[19] M.-H. Horng, Y.-N. Sun, and X.-Z. Lin, ''Texture feature coding method for classification of liver sonography,'' *Computerized Med. Imag. Graph.*, vol. 26, no. 1, pp. 33–42, Jan. 2002.

[20] J. Santos, J. S. Silva, A. A. Santos, and P. Belo-Soares, ''Detection of pathologic liver using ultrasound images,'' *Biomed. Signal Process. Control*, vol. 14, pp. 248–255, Nov. 2014.

[21] G. Qiu, S. Huang, and Y. Gu, ''Experimental investigation and multi-conditions identification method of centrifugal pump using Fisher discriminant ratio and support vector machine,'' *Adv. Mech. Eng.*, vol. 11, no. 9, 2019, Art. no. 1687814019878041.

[22] X. Zeng, M. Naghedolfeizi, S. Arora, and D. Aberra, ''Selection of principal components based on Fisher discriminant ratio,'' *Proc. SPIE*, vol. 9871, May 2016, Art. no. 98710K.

[23] A. Gaber, G. Attiya, A. Hamdy, and T. Elsayed, ''Recognition of diffuse liver cirrhosis based on image analysis,'' *Imag. Sci. J.*, vol. 64, no. 3, pp. 152–159, Apr. 2016.

[24] M. Owjimehr, H. Danyali, M. S. Helfroush, and A. Shakibafard, ''Staging of fatty liver diseases based on hierarchical classification and feature fusion for back-scan–converted ultrasound images,'' *Ultrason. Imag.*, vol. 39, no. 2, pp. 79–95, Mar. 2017.

[25] A. Andrade, J. S. Silva, J. Santos, and P. Belo-Soares, ''Classifier approaches for liver steatosis using ultrasound images,'' *Procedia Technol.*, vol. 5, pp. 763–770, Jan. 2012.

[26] M. Singh, S. Singh, and S. Gupta, ''An information fusion based method for liver classification using texture analysis of ultrasound images,'' *Inf. Fusion*, vol. 19, pp. 91–96, Sep. 2014.

[27] S. Wang, D. Li, X. Song, Y. Wei, and H. Li, ''A feature selection method based on improved Fisher's discriminant ratio for text sentiment classification,'' *Expert Syst. Appl.*, vol. 38, no. 7, pp. 8696–8702, Jul. 2011.

AHMED GABER MABROUK received the B.Sc. and M.Sc. degrees in computers and systems engineering from Menouf University, Egypt. He is currently pursuing the Ph.D. degree in computers engineering with Minia University. He is currently a Researcher with Minia University and also an Assistant Lecturer with the High Institute for Computers and Information Systems. His main research interests include image analysis, image processing, pattern analysis, machine learning, and deep learning.

ALAA HAMDY received the B.Sc. and M.Sc. degrees in computer engineering from Helwan University, in 1996, and the Ph.D. degree from the Faculty of Electrical Engineering, Poznan University of Technology, Poland, in 2004. He was commissioned by the Ministry of Higher Education to write a book for the Technical Colleges. He was a Member of the Group of the Information Technology Center (ITC), University of Helwan. He is a Representative of the Department with the Faculty of Engineering, Electronic Coordination Office. He is currently working as an Associate Professor with the Faculty of Engineering, Helwan University. He is the author/a coauthor of more than 40 scientific publications. His research interests include image processing, pattern analysis, and machine vision. He has been serving as an Academic Member for the Review Board Team of two high-impact factor international journals.

HAMMAM M. ABDELAAL received the B.Sc. and M.Sc. degrees in computers and systems engineering from Al-Azhar University, and the Ph.D. degree in computer engineering, Minia University, Egypt. He is currently a Lecturer with the Higher Institute for Computers and Information Systems, New Cairo. He is the author/a coauthor of different scientific publications. His main areas of research interests include machine learning techniques, supervised learning algorithms, natural languages processing, and data mining. He has been serving as a Reviewer for high-impact factor international journals.

AHMED GAMAL ELKATTAN received the master's degree from the Business Administration Department, Cairo University. He is currently an Assistant Lecturer with the Faculty of Administrative Sciences, King Salman International University (KSIU), Egypt. He is also an International Certified Instructor with the Huawei Academy in artificial intelligence (AI) and cutting-edge technologies. His research interests include artificial intelligence, machine learning, sharing economy, transformative service research (TSR), and consumers' well-being. He has accumulated expertise in many statistical software packages, such as SPSS, AMOS and SmartPLS; and programming packages such as Python.

MOTASEM M. ELSHOURBAGY received the B.Sc. and master's degreesfrom the Communication and Electronics Department, Faculty of Engineering, Helwan University, Cairo, Egypt, in 2001 and 2007, respectively, and the Ph.D. degree in computer engineering from the Computer Engineering Department, Faculty of Engineering, Cairo University, Cairo, in 2016. He has been a Doctor (Lecturer) with the Faculty of Engineering at Mataria, since 2016. He is working as a Doctor of Computer Engineering with the Faculty of Engineering at Mataria, Helwan University. His research interests include image processing, computer vision, machine learning, deep learning, and artificial intelligence.

HASSAN A. YOUNESS ALANSARY (Member, IEEE) received the B.Sc. and M.Sc. degrees from Assiut University, Assiut, Egypt, and the Ph.D. degree from the Graduate School of Information Science and Technology, Osaka University, Japan, with the cooperation of Ain Shams University, Egypt. He worked for IBM Company and Mentor Graphics, Egypt. He is currently an Associate Professor with Minia University, and also the Chairman of the Computers and Systems Engineering Department. His research interests include integrated system design, fault tolerance, HW/SW co-design, parallel computers, embedded systems, GPGPU, APU and MPSoCs, homogeneous/heterogeneous systems, machine learning, deep learning, and AI.